Journal of Cerebral Blood Flow & Metabolism
23:395–398 © 2003 The International Society for Cerebral Blood Flow and Metabolism
Published by Lippincott Williams & Wilkins, Inc., Philadelphia

Short Communication

Cyclooxygenase-2 Expression Associated With Spreading Depression in a Primate Model

*Chiaki Yokota, †Hiroyasu Inoue, ‡Yuji Kuge, §Takeo Abumiya, ‖Masafumi Tagaya, ¶Yasuhiro Hasegawa, #Norimasa Ejima, **Nagara Tamaki, and ¶Kazuo Minematsu

**Cerebrovascular Laboratory, Department of Pathogenesis, and †Department of Pharmacology, National Cardiovascular Center Research Institute, Departments of ‡Tracer Kinetics and **Nuclear Medicine, Graduate School of Medicine, Hokkaido University §Department of Neurosurgery, Ebetu Hospital, ‖Department of Medicine, National Osaka Hospital, ¶Cerebrovascular Division, Department of Medicine, National Cardiovascular Center, and #Institute for Biofunctional Research Co., Inc., Osaka, Japan*

Summary: The authors previously provided evidence that spreading depression (SD) can be evoked in primates. Cyclooxygenase-2 (COX-2) expression has been found to increase in the rodent cortex undergoing SD, and the authors sought to determine whether this association exists in primate brain. In the present study, neuronal COX-2 expression was induced during SD in the primate cortex. The mean expression ratio of COX-2 messenger RNA in animals with SD was significantly higher than that measured in controls (*1.69 vs. 0.5*; $P \approx 0.02$). Induction of COX-2 in these animals was also detected by human microarray analysis. Results show that, as in rodents, neuronal COX-2 is induced in the primate cortex in response to SD. **Key Words:** Spreading depression—Cyclooxygenase-2—Microarray analysis—Primate.

Cortical spreading depression (SD), the reversible depression of cortical electrical activity, plays a role in the development of cerebral ischemic injury and migraine (Lauritzen et al., 1983; Olesen et al., 1981; Woods et al., 1994). Repetitive, pathologic SDs were similarly found to play a role in the development of ischemic injury under conditions of focal brain ischemia in rats (Gill et al., 1992; Hossmann, 1994; Iijima et al., 1992; Takano et al., 1996). Changes in cerebral blood flow (CBF) in experimental SD models in rats and cats were characterized by transient focal cortical hyperemia, followed by persistent hypoperfusion (Kuge et al., 2000; Lauritzen et al., 1982; Piper et al., 1991). Recently, we provided the first direct evidence that SD, accompanied by focal cortical hyperemia, can be evoked in primates (Yokota et al., 2002). The long-lasting hypoperfusion that followed this hyperemia in rats and cats has not been observed in primates.

The gene for cyclooxygenase-2 (COX-2), a rate-limiting enzyme in prostaglandin synthesis, was induced in the nonprimate cortex during SD (Koistinaho et al., 1999; Miettinen et al., 1997). Cyclooxygenase-2 appeared to mediate the increase in CBF produced by synaptic activity in the somatosensory cortex in mice (Niwa et al., 2000). The contribution of SD and its associated genes to the pathogenesis of human brain diseases has not been elucidated.

As a first step in determining which genes show altered expression during SD in primates, we examined whether the COX-2 gene was upregulated. Using a human complementary DNA (cDNA) array system, we also examined the effect of SDs on gene-expression profiles.

MATERIALS AND METHODS

Spreading depression model and brain preparation

Nine adult, male cynomolgus monkeys were divided into two groups: a normal control group (group C, $n = 3$) and a group in which SD was evoked by applying 3.3-mol/L KCl to

Received September 18, 2002; final version received December 9, 2002; accepted December 9, 2002.

This study was supported in part by Special Coordination Funds for Promoting Science and Technology (Strategic Promotion System for Brain Science) from the Ministry of Education, Culture, Sports, Science and Technology of Japan, by a Grant-in-Aid for Scientific Research from the Japan Society for the Promotion of Science, by a grant from the Takeda Medical Research Foundation in Japan, and by a Japan Heart Foundation Research Grant.

Address correspondence and requests to Dr. Yokota, Cerebrovascular Laboratory, National Cardiovascular Center Research Institute, 5-7-1 Fujishirodai, Suita, Osaka 565-8565, Japan; e-mail: cyokota@ri.ncvc.go.jp

DOI: 10.1097/01.WCB.0000055293.67563.2E

the cortex (group SD, n = 6). All procedures were approved by our Institutional Animal Research Committee and were performed in accordance with standards published by the National Research Council in the *Guide for the Care and Use of Laboratory Animals*.

Shifts of direct current potential were measured in four animals in the SD group only with a microelectrode placed just rostral to the chemical stimulation site; a single episode was recorded in three animals, and six episodes were recorded in one animal. Direct current potential was measured in the remaining two animals with a microelectrode that was placed caudal to the chemical stimulation site as well as with microelectrodes placed rostral to the chemical stimulation site; one of these animals was subjected to eight recording episodes at this site, whereas the remaining animal was subjected to two direct current shifts, each of which was recorded from a point that was rostrally adjacent to the chemical stimulation site, as well as to six episodes at the caudal site.

Two hours after KCl application, the brains from these animals were perfused with cold saline, after which the animals were killed and the brains removed. Several samples from each cortex were harvested and stored at −80°C until use, whereas other samples were embedded in paraffin.

RNA blot analysis

RNA preparation and blot analysis were performed as previously described (Inoue et al., 1995). Cyclooxygenase-2 messenger RNA (mRNA) in each region was expressed as the ratio of the COX-2 mRNA signal to the GAPDH mRNA signal in that region (expression ratio).

Microarray analysis

Microarray analysis was conducted using Genome System (St. Louis, MO, U.S.A.) as described elsewhere (Lyer et al., 1999). The microarray contained 9,182 elements: 8,412 unique annotated genes or expressed sequence tags, and 4,757 characterized human protein genes. Left cortical RNAs from the SD (>5 episodes; n = 3) and control (n = 3) groups were pooled. Poly $(A)^+$ RNAs were purified from these RNAs using oligo$(dT)_{30}$-latex (Takara, Inc., Shiga, Japan) to use as templates for cDNA synthesis. The cDNA probes were reverse transcribed with 5'Cy3 or fluorescently labeled Cy5 and were hybridized with Human UniGEM V (version 2.0). The average of the total Cy3 and Cy5 signals yielded a ratio that was used to normalize the signals.

Immunoblot analyses

Left temporal cortical samples were weighed and homogenized in 10 volumes of cold 62.5-mmol/L Tris buffer (pH 6.8) containing 1% sodium dodecylsulfate, 10% glycerin, and 5% 2-mercaptoethanol. Tissue homogenates were heated to 90°C for 5 minutes and then centrifuged at 15,000*g* for 10 minutes at 4°C. The supernatants were separated by SDS-PAGE (5% to 20% acrylamide gradient) and proteins transferred onto a nitrocellulose sheet. The blots were incubated with anti–COX-2 antibody (dilution 1:1,000; Cayman Chemical, Ann Arbor, MI, U.S.A.) for 1 h at 25°C and were then washed in 50-mmol/L phosphate-buffered saline (pH 7.4) containing 0.05% Tween 20.

Immunohistochemistry

A mirror-sectioning technique was used to colocalize COX-2 and microtubule-associated protein 2 (MAP-2), a neuronal skeletal protein. Deparaffinized temporal cortical sections (3 μm) were incubated with a polyclonal anti–COX-2 antibody (dilution 1:100; Cayman Chemical) and a monoclonal anti–MAP-2 antibody (clone HM-2; dilution 1:2,400; Sigma, St. Louis, MO, U.S.A.) overnight at 4°C. The sections were washed with phosphate-buffered saline, and biotinylated goat anti–rabbit immunoglobulin (Vector Laboratories, Burlingame, CA, U.S.A.) or biotinylated $F(ab')_2$ rabbit anti–mouse immunoglobulin (dilution 1:500; Dako, Carpinteria, CA, U.S.A.) was applied to the sections, which were then incubated for 30 minutes at 25°C. Labeling was visualized using a Vectastain Elite Kit (Vector Laboratories).

Statistical analysis

Data are expressed as the mean ± standard deviation. Comparisons of COX-2 mRNA expression between groups were made using the Mann-Whitney *U* test. A two-tailed *P* value less than 0.05 was considered to be significant.

RESULTS

Expression of cyclooxygenase-2 mRNA

Cyclooxygenase-2 mRNA expression increased in the cortex in which SD was induced (left) compared with both the contralateral side and the left cortex in group C (Fig. 1A). The expression ratio of COX-2 mRNA in the left cortex in the SD group (1.69 ± 0.57) was significantly greater ($P = 0.02$) than in the left cortex in group C (0.5 ± 0.05; Fig. 1B).

Cyclooxygenase-2 localization

Immunoblots revealed a 70- to 72-kd COX-2–immunoreactive band (Gidlund et al., 1981) in tissue derived from the SD group, which was barely detectable in group C (Fig. 1C). Immunoreactive neurons were observed in animals that received six SD episodes rostral to the chemical stimulation site (Fig. 1D). Immunoreactive MAP-2 was demonstrable in the same neurons that displayed COX-2 immunoreactivity.

Gene-expression patterns

Increases in normalized gene-expression signals above 1.5-fold were observed for two genes among a total 9,182 elements: the COX-2 (1.6-fold) and basic transcription element–binding protein 1 (1.6-fold) genes. Twenty-one elements were found to be different by at least 1.4-fold. Figure 2 shows representative images of scanned arrays hybridized with left cortical samples.

DISCUSSION

Previous studies have suggested that COX-2 plays a role in the development of ischemic injury during focal brain ischemia in rodents (Collaco-Moraes et al., 1996;

FIG. 2. Gene-expression patterns in the brains of animals in the spreading depression (SD) and control (C) groups. Representative images of scanned arrays hybridized with cortical samples from C and SD animals are shown. Of the 9,182 elements that were examined, expression of the cyclooxygenase-2 gene (red circles) was found to be increased by 1.6-fold in the SD group.

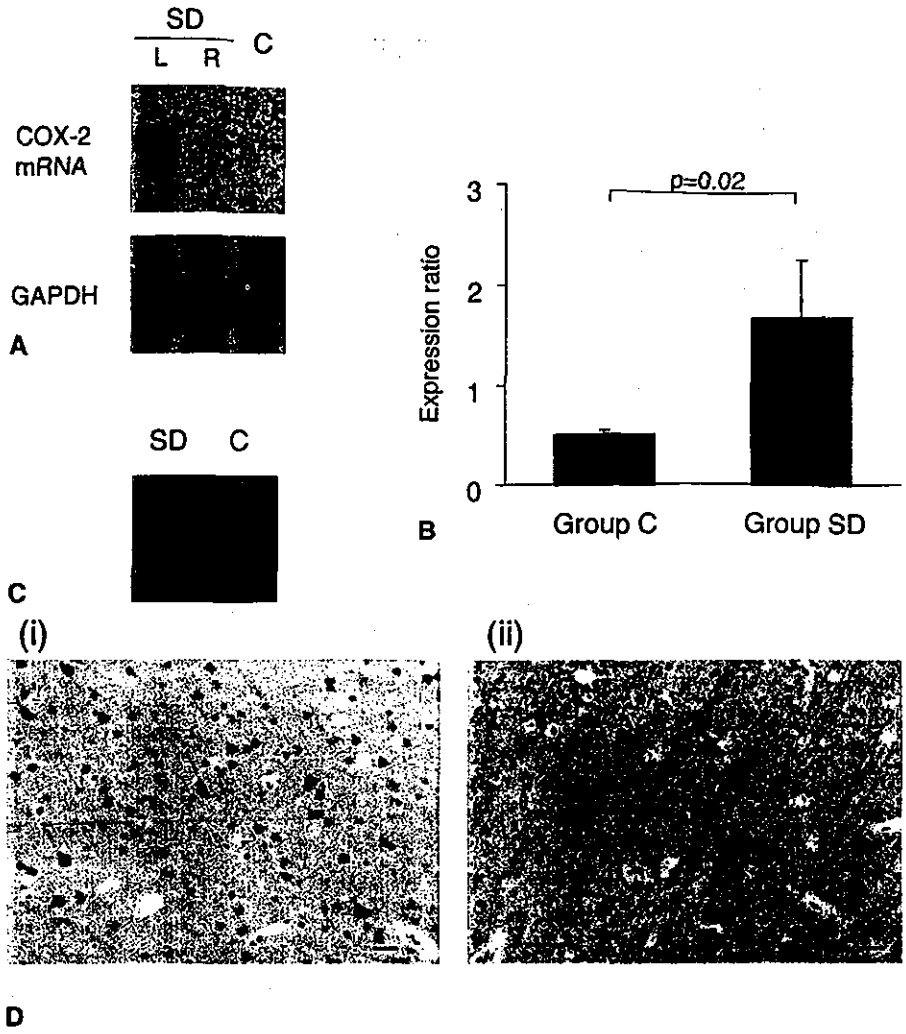

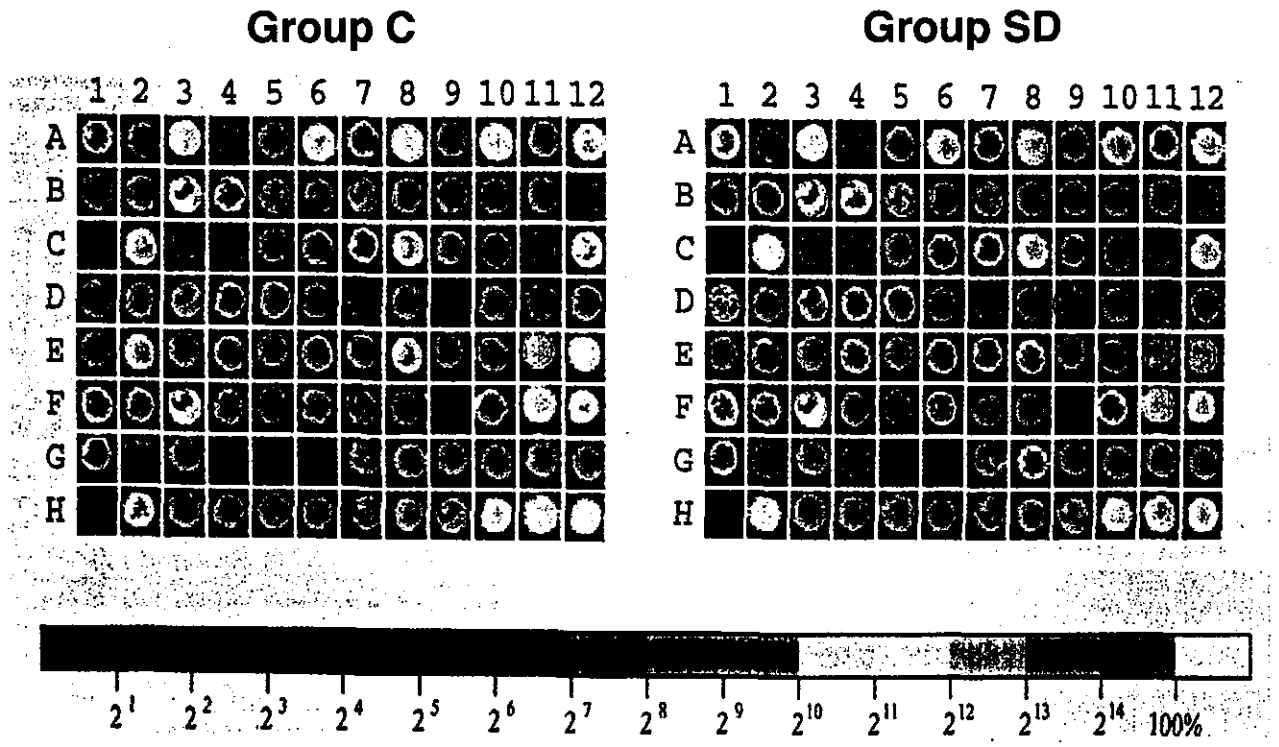

FIG. 1. Cyclooxygenase-2 (COX-2) expression in the primate brain. **(A)** Autoradiograms of COX-2 (top) and glyceraldehyde-3-phosphate dehydrogenase (GAPDH) messenger RNA (bottom) from normal (group C) and spreading depression (SD) animals (group SD). Note that induced COX-2 expression was prominent in the left cortical samples (ipsilateral to the side in which SD was induced). COX-2 expression in the contralateral cortices and in control samples (group C) was faint. **(B)** Expression ratios of COX-2 in each group. The expression ratio of the cortex ipsilateral to the cortex in which SD was induced was significantly higher than that measured in group C ($P = 0.02$). **(C)** Immunoblot analysis revealed a 70- to 72-kd COX-2–immunoreactive band that is clearly seen in the SD group but that is barely detectable in group C. **(D)** Mirror section images immunostained for COX-2 (i) and microtubule-associated protein 2 (MAP-2; ii) are shown. Immunoreactive COX-2 and MAP-2 were localized in the same neurons; cell bodies and apical dendrites showed immunoreactivity. Scale bars: 200 μm.

Nogawa et al., 1997) and that prevention of COX-2 expression might be beneficial in treating human ischemic stroke. Ischemia-related SDs have been regarded as good targets for pharmacologic intervention in stroke because they exacerbate the preexisting energy depletion in the periinfarct zone (Hossmann, 1994; Takano et al., 1996). Cyclooxygenase-2 was induced after SD and as a result of focal brain ischemia in rat models (Koistinaho et al., 1999; Miettinen et al., 1997). Koistinaho and Chan (2000) reported that SD directly induced COX-2 expression in focal brain ischemia by stimulating the NMDA receptor and activating phospholipase A_2. Only a few postmortem studies, however, reported COX-2 expression in human brain ischemia (Iadecola et al., 1999; Sairanen et al., 1998).

In our study, COX-2 was induced in the cortices that experienced SD, supporting previous observations in rodents (Koistinaho et al., 1999; Miettinen et al., 1997). Cyclooxygenase-2 gene expression increased by 1.6-fold in the SD group, as detected using a DNA microarray. The gene transcribing basic transcription element–binding protein 1, a thyroid hormone–regulated gene found in the developing rat brain, was also upregulated (Cayrou et al., 2002); the relation between this protein and SD remains to be clarified. Enard et al. (2002) showed numerous quantitative differences in gene expression between closely related mammalian species. Because they showed that such differences were particularly pronounced in the human brain, primate cDNA arrays analysis will need to be improved before we can fully identify candidate genes that may be involved in SD. In summary, as in rodents, neuronal COX-2 is induced in the primate cortex in response to SD.

Acknowledgments: The authors thank Dr. Toshiho Ohtsuki for his scientific input.

REFERENCES

Cayrou C, Denver RJ, Puymirat J (2002) Suppression of the basic transcription element–binding protein in brain neuronal cultures inhibits thyroid hormone-induced neurite branching. *Endocrinology* 143:2242–2249

Collaco-Moraes Y, Aspey B, Harrison M, Belleroche JD (1996) Cyclooxygenase-2 messenger RNA induction in focal cerebral ischemia. *J Cereb Blood Flow Metab* 16:1366–1372

Enard W, Khaitovich P, Klose J, Zollner S, Heissig F, Giavalisco P, Niselt-Struwe K, Muchmore E, Varki A, Ravid R, Doxiadis GM, Bontrop RE, Paabo S (2002) Intra- and interspecific variation in primate gene expression patterns. *Science* 296:340–343

Gidlund M, Orn A, Pattengale PK, Jansson M, Wigzell H, Nilsson K (1981) Natural killer cells kill tumor cells at a given stage of differentiation. *Nature* 292:848–850

Gill R, Andine P, Hillered L, Persson L, Hagberg H (1992) The effect of MK-801 on cortical spreading depression in the penumbral zone following focal ischemia in the rat. *J Cereb Blood Flow Metab* 12:371–379

Hossmann KA (1994) Viability thresholds and the penumbra of focal ischemia. *Ann Neurol* 36:557–565

Iadecola C, Forster C, Nogawa S, Clark HB, Ross ME (1999) Cyclooxygenase-2 immunoreactivity in the human brain following cerebral ischemia. *Acta Neuropathol* 98:9–14

Iijima T, Mies G, Hossmann KA (1992) Repeated negative DC deflections in rat cortex following middle cerebral artery occlusion are abolished by MK-801: effect on volume of ischemic injury. *J Cereb Blood Flow Metab* 12:727–733

Inoue H, Yokoyama C, Hara S, Tone Y, Tanabe T (1995) Transcriptional regulation of human prostaglandin-endoperoxide synthase-2 gene by lipopolysaccharide and phorbol ester in vascular endothelial cells. *J Biol Chem* 270:24965–24971

Koistinaho J, Chan PH (2000) Spreading depression-induced cyclooxygenae-2 expression in the cortex. *Neurochem Res* 25:645–651

Koistinaho J, Pasonen S, Yrjanheikki J, Chan PH (1999) Spreading depression-induced gene expression is regulated by plasma glucose. *Stroke* 30:114–119

Kuge Y, Hasegawa Y, Yokota C, Minematsu K, Hashimoto N, Miyake Y, Yamaguchi T (2000) Effects of single and repetitive spreading depression on cerebral blood flow and glucose metabolism in cats: a PET study. *J Neurol Sci* 176:114–123

Lauritzen M, Jorgensen MB, Diemer NH, Gjedde A, Hansen AJ (1982) Persistent oligemia of rat cerebral cortex in the wake of spreading depression. *Ann Neurol* 12:469–474

Lauritzen M, Olsen TS, Lassen NA, Paulson OB (1983) Changes in regional cerebral blood flow during the course of classic migraine attacks. *Ann Neurol* 13:633–641

Lyer VR, Eisen MB, Ross DT, Schuler G, Moore T, Lee JCF, Trent JM, Staudt LM, Hudson J, Boguski MS, Lashkari D, Shalon D, Botstein D, Brown PO (1999) The transcriptional program in the response of human fibroblasts to serum. *Science* 283:83–87

Miettinen S, Fusco FR, Yrjanheikki J, Keinanen R, Hirvonen T, Roivainen R, Narhi M, Hokfelt T, Koistinaho J (1997) Spreading depression and focal brain ischemia induce cyclooxygenase-2 in cortical neurons through *N*-methyl-D-aspartic acid-receptors and phospholipase A_2. *Proc Natl Acad Sci U S A* 94:6500–6505

Niwa K, Araki E, Morham SG, Ross ME, Iadecola C (2000) Cyclooxygenase-2 contributes to functional hyperemia in whisker-barrel cortex. *J Neurosci* 20:763–770

Nogawa S, Zhang F, Ross ME, Iadecola C (1997) Cyclo-oxygenase-2 gene expression in neurons contributes to ischemic brain damage. *J Neurosci* 17:2746–2755

Olesen J, Larsen B, Lauritzen M (1981) Focal hyperemia followed by spreading oligemia and impaired activation of rCBF in classic migraine. *Ann Neurol* 9:344–352

Piper RD, Lambert GA, Duckworth JW (1991) Cortical blood flow changes during spreading depression in cats. *Am J Physiol* 261:H96–H102

Sairanen T, Ristimaki A, Karjalainen-Lindsberg M-L, Paetau A, Kaste M, Lindsberg PJ (1998) Cyclooxygenase-2 induced globally in infarcted human brain. *Ann Neurol* 43:738–747

Takano K, Latour LL, Formato JE, Carano RAD, Helmer KG, Hasegawa Y, Sotak CH, Fisher M (1996) The role of spreading depression in focal ischemia evaluated by diffusion mapping. *Ann Neurol* 39:308–318

Woods RP, Iacoboni M, Mazziotta JC (1994) Bilateral spreading cerebral hypoperfusion during spontaneous migraine headache. *New Engl J Med* 331:1689–1692

Yokota C, Kuge Y, Hasegawa Y, Tagaya M, Abumiya T, Ejima N, Tamaki N, Yamaguchi T, Minematsu K (2002) Unique profile of spreading depression in a primate model. *J Cereb Blood Flow Metab* 22:835–842

Cerebral Hemodynamic Evaluation Using Perfusion-Weighted Magnetic Resonance Imaging

Comparison With Positron Emission Tomography Values in Chronic Occlusive Carotid Disease

Katsufumi Kajimoto, MD; Hiroshi Moriwaki, MD; Naoaki Yamada, MD; Kohei Hayashida, MD; Junya Kobayashi, MD; Kotaro Miyashita, MD; Hiroaki Naritomi, MD

Background and Purpose—Perfusion-weighted magnetic resonance imaging (PWI) is a reliable and semiquantitative method for estimating cerebral hemodynamics. We sought to evaluate the potential of PWI for assessing cerebral blood flow (CBF) and metabolism compared with positron emission tomography (PET) in patients with chronic occlusive carotid disease.

Methods—In 24 patients with chronic unilateral occlusive carotid disease, time-to-peak (TTP) delay (TTP-D) measured by PWI was compared with CBF, cerebral blood volume (CBV), and oxygen extraction fraction (OEF) obtained by PET. TTP indicates the time from the start of PWI to the bolus peak. TTP-D indicates the difference in TTP values between the occlusive and contralateral hemispheres. TTP-D was compared between patients with normal and reduced CBF/CBV and also between patients with normal and elevated OEF.

Results—TTP-D in patients with reduced CBF/CBV was significantly longer than that in patients with normal CBF/CBV (3.4±1.8 versus 1.4±0.7 seconds; $P<0.001$). In the patients with reduced CBF/CBV, TTP-D correlated with OEF significantly ($r=0.710$, $P<0.0001$). TTP-D in patients with elevated OEF was significantly longer than that in patients with normal OEF (4.8±2.2 versus 2.0±0.9 seconds; $P<0.01$). In all 5 patients with TTP-D ≥4 seconds, OEF was elevated markedly.

Conclusions—TTP-D ≥4 seconds is considered to indicate a high risk of hemodynamic failure. The measurement of TTP-D by PWI appears to provide important clinical information for evaluating cerebral hemodynamics in chronic occlusive carotid disease. (***Stroke*. 2003;34:1662-1666.)**

Key Words: carotid artery occlusion ■ hemodynamics ■ magnetic resonance imaging, perfusion-weighted ■ tomography, emission computed

Perfusion-weighted magnetic resonance imaging (PWI) provides information on the hemodynamic status of tissue and can detect impaired perfusion in both the ischemic core and the surrounding brain regions.[1] Quantification of cerebral blood flow (CBF) and cerebral blood volume (CBV) with PWI is enabled by applying indicator dilution theory.[2-7] However, the indicator dilution method requires measurements of the arterial contrast agent concentration as an arterial input function (AIF), which is a demanding and complicated process in the daily clinical setting. Time-to-peak (TTP) value can be estimated readily and rapidly with PWI. TTP images further permit us to obtain another hemodynamic parameter, TTP delay (TTP-D), which is the difference between the TTP in the target hemisphere and in the contralateral hemisphere.

Several studies compared results of PWI and those of established hemodynamic imaging techniques.[5,6,8-10] To the best of our knowledge, however, there have been no clinical studies comparing PWI with positron emission tomography (PET), a gold standard of perfusion imaging technique, in chronic occlusive carotid disease.

The aim of this study was to evaluate the potential of TTP-D for assessing cerebral hemodynamics, including cerebral metabolism, in comparison with PET parameters in patients with chronic occlusive carotid disease. We chose stroke patients with chronic unilateral carotid occlusive disease as our subjects because they offer a stable experimental population.

Subjects and Methods

Subjects

Between June 2000 and May 2002, a total of 37 consecutive patients with chronic cerebrovascular diseases were examined with both PWI and PET in the same period in our department (Department of

Received January 21, 2003; accepted February 5, 2003.

From the Departments of Cerebrovascular Medicine (K.K., H.M., J.K., K.M., H.N.) and Radiology and Nuclear Medicine (N.Y., K.H.), National Cardiovascular Center, Osaka, Japan.

Reprint requests to Katsufumi Kajimoto, MD, Department of Cerebrovascular Medicine, National Cardiovascular Center, 5-7-1 Fujishirodai, Suita City, Osaka 565-8565, Japan. E-mail kkajimot@hsp.ncvc.go.jp.

Stroke is available at http://www.strokeaha.org

DOI: 10.1161/01.STR.0000076014.60026.45

Patient Characteristics, MRA, and Angiographic Findings

Patient No.	Lesion Site	Age/Sex	Clinical Feature	Collateral Routes
1	RICO	50/M	Minor stroke	Circle of Willis
2	RICO	56/M	Minor stroke	Circle of Willis
3	RICO	66/M	Minor stroke	Circle of Willis
4	RICO	71/M	Minor stroke	Circle of Willis
5	RICO	78/M	Minor stroke	Circle of Willis
6	RICO	62/M	TIA	Circle of Willis
7	RICO	64/M	TIA	Circle of Willis
8	RICO	60/M	Asymptomatic	Circle of Willis
9	RICO	74/M	Asymptomatic	Circle of Willis
10	LICO	67/F	Minor stroke	Circle of Willis
11	LICO	75/M	Minor stroke	Circle of Willis
12	LICO	66/M	Minor stroke	Leptomeningeal
13	LICO	72/M	TIA	Circle of Willis
14	LICO	82/M	TIA	Circle of Willis
15	LICO	63/M	Asymptomatic	Circle of Willis
16	LICO	78/M	Asymptomatic	Circle of Willis
17	RICS	69/M	Minor stroke	...
18	RICS	83/F	TIA	...
19	RICS	71/F	Asymptomatic	...
20	RMCO	65/F	Minor stroke	Leptomeningeal
21	RMCO	67/M	Minor stroke	Leptomeningeal
22	LMCO	82/F	Minor stroke	Leptomeningeal
23	LMCO	65/M	Asymptomatic	Leptomeningeal
24	LMCS	67/M	Minor stroke	...

R indicates right; L, left; ICO, internal carotid artery occlusion; ICS, internal carotid artery stenosis; MCO, middle cerebral artery occlusion; MCS, middle cerebral artery stenosis; TIA, transient ischemic attack.

Cerebrovascular Medicine). From these patients, 24 patients (19 men and 5 women; mean age, 68.9±8.2 years; age range, 50 to 83 years) meeting the following criteria were selected as subjects studied: (1) major cerebral artery, such as the internal carotid artery (ICA) or the main trunk of the middle cerebral artery (MCA), is occluded or narrowed (≥75%) unilaterally; and (2) vascular lesion is atherosclerotic in nature. The other 13 patients were excluded from the study because of the following reasons: (1) the major cerebral arteries in the contralateral carotid system were also occluded or narrowed significantly (≥50%) (n=4); (2) the stenosis of the affected side was not sufficiently severe in degree (<75%) (n=7); or (3) the vascular lesions were attributable to nonatherosclerotic diseases, such as moyamoya disease (n=2). Sixteen patients had unilateral ICA occlusion, 3 had unilateral ICA stenosis, 4 had unilateral MCA (M1) occlusion, and 1 had unilateral MCA (M1) stenosis (Table). All patients were evaluated >4 weeks after the latest clinical episode. Vascular lesions were evaluated by digital subtraction angiography (DSA) in 12 patients and by MR angiography in the other 12 patients. Thirteen patients had minor stroke, 5 had transient ischemic attack (TIA), and 6 were asymptomatic. The definitions of TIA and minor stroke were based on standardized criteria.[11] TIA was diagnosed clinically in patients with focal neurological symptoms relating to focal cerebral, brain stem, or retinal ischemia with abrupt onset and complete resolution within 24 hours. Minor completed stroke was defined as Rankin Scale score 1 or 2. All patients underwent PWI and PET in the same period (interval, 0 to 12 days; mean, 3.5±3.1 days). There were no symptomatic changes in any patients during the period between PWI and PET. Informed consent was obtained from all patients after a detailed explanation of the purpose of the study and the scanning procedure was provided.

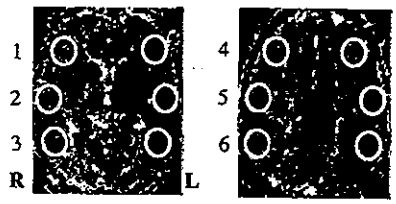

Figure 1. ROIs used for the analysis of hemodynamic state. Two tomographic planes including the basal ganglia and centrum semiovale are selected for analyses of PWI and PET data. On each imaging plane, circular ROIs with 16-mm diameters are placed manually in the MCA area of the occlusive hemisphere. ROIs are also placed in the homologous regions of the contralateral MCA area to calculate TTP-D. R indicates right; L, left.

MRI Protocol

MRI was performed with the use of a clinical 1.5-T whole-body MR system with a conventional gradient system (Magnetom Vision, Siemens Medical System). Before PWI studies, conventional MR images, including T2-weighted, T1-weighted, and fluid-attenuated inversion recovery (FLAIR) images, were acquired with a spin-echo pulse sequence. PWI was acquired with T2*-weighted imaging; gradient-echo, echo-planar imaging had the following parameters: slice number 10, slice thickness 4 mm, repetition time 2000 ms, echo time 60 ms, field of view 230 mm, and matrix 128×128. PWI was repeated 40 times every 2 seconds. A contrast agent of 0.1 mmol/kg gadolinium-DTPA was injected through an antecubital vein with a 22-gauge cannula at a rate of 3 to 4 mL/s followed by 20 mL saline. All images including TTP were calculated automatically on the host computer of the MR system. TTP refers here to the time between the start of PWI and the bolus peak.[12] TTP-D was calculated as TTP in the occlusive hemisphere subtracted from that in the contralateral hemisphere.

PET Protocol

PET measurements were performed during the same period as MRI in all the patients. CBF, CBV, cerebral metabolic rate for oxygen ($CMRO_2$), and oxygen extraction fraction (OEF) were obtained with a Headtome IV PET scanner (Shimadzu) with a spatial resolution of 4.5 mm full width at half maximum and the ^{15}O-labeled gas inhalation technique.[13] In brief, an emission scan with an external ^{68}Ge-^{68}Ga ring source was corrected for the effects of tissue attenuation with the use of corresponding transmission scans. After transmission scanning, the separate scans were performed during continuous inhalation of ^{15}O-labeled carbon dioxide ($C^{15}O_2$) and molecular oxygen ($^{15}O_2$) for the measurements of CBF and OEF, respectively. The third scan, for the measurement of CBV, was performed after 2-minute inhalation of ^{15}O-labeled carbon monoxide ($C^{15}O$).[14] During the scans, blood samples were obtained serially for measuring arterial isotope activities, arterial oxygen content (O_2C), and arterial Pco_2. $CMRO_2$ was calculated as $CBF \times OEF \times O_2C$.

Data Analysis

Two planes, including the basal ganglia and centrum semiovale, were chosen for analyses of PWI and PET data. On each imaging plane, circular regions of interest (ROIs) with 16-mm diameters were placed manually on the MCA area of the occlusive side (Figure 1). ROI was also placed on the homologous regions of the contralateral side for references to measure TTP-D. We measured TTP-D in each ROI. The mean value of all hemispheric ROIs was cited to represent the hemodynamic state in the occlusive hemisphere. Of all the 144 ROIs, 4 ROIs within the infarcted areas were excluded from the analysis. The regional values in the remaining 140 ROIs and the mean hemispheric values in 24 occlusive hemispheres were subjected to the analyses. Normal values of PET parameters were obtained from healthy volunteers, as published previously.[15] CBF/CBV values ≤10.8, the mean minus 2 SD of normal values, were judged to indicate abnormally reduced CBF/CBV. Likewise, OEF

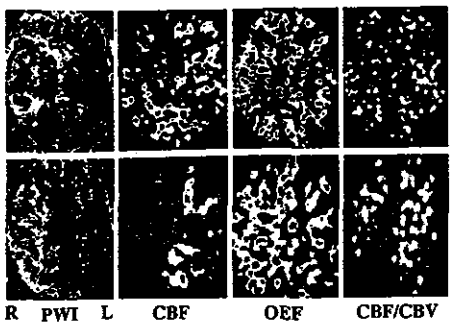

Figure 2. PWI and PET findings in patient 1 with right ICA occlusion. PWI shows delayed perfusion in the entire territory of the right (R) hemisphere, with a mean TTP-D of 5.3 seconds. PET demonstrates decreased CBF, elevated OEF, and reduced CBF/CBV in the right hemisphere. L indicates left.

values ≥0.52, the mean plus 2 SD of normal values, were cited to indicate abnormally elevated OEF.

Statistical Analysis

Results are presented as mean±SD. Relations between TTP-D obtained by PWI and CBF/CBV obtained by PET were evaluated with logarithmic regression analysis. Relations between TTP-D obtained by PWI and OEF obtained by PET were evaluated with linear regression analysis. The patients were divided into 2 groups by the mean hemispheric CBF/CBV: group A (n=9) with normal CBF/CBV (>10.8) and group B (n=15) with reduced CBF/CBV (≤10.8). The patients were also classified into another 2 groups by the mean hemispheric OEF: group α (n=18) with normal OEF (<0.52) and group β (n=6) with elevated OEF (≥0.52). The difference in the TTP-D between groups A and B or between groups α and β was analyzed with a Mann-Whitney *U* test. A probability value of <0.05 was considered significant.

Results

In a representative case, a 50-year-old man (patient 1) developed left hemiparesis and dysarthria. DSA demonstrated right ICA occlusion. FLAIR images revealed subcortical infarctions in the right centrum semiovale and frontal white matter. PWI showed delayed perfusion throughout the right hemisphere. The mean TTP-D value in the right hemisphere was markedly prolonged to 5.3 seconds. PET demonstrated severely decreased CBF, moderately decreased $CMRO_2$, elevated OEF, and reduced CBF/CBV in the right hemisphere. Mean values of OEF and CBF/CBV in the right hemisphere were 0.54 and 8.17, respectively (Figure 2).

As shown in the Table, the occlusive hemisphere was supplied by anterograde collateral circulation via the anterior or posterior communicating artery in 15 of 16 patients with ICA occlusion. Retrograde circulation via leptomeningeal arteries was observed in 1 patient with ICA occlusion and in all 4 patients with MCA occlusion.

Figure 3 shows the relation between TTP-D and CBF/CBV in all 140 ROIs. There was a significant correlation between the 2 parameters (r=0.411, P<0.0001). TTP-D values in group B were significantly prolonged compared with those in group A (3.4±1.8 versus 1.4±0.7 seconds; P<0.001) (Figure 4A). In 13 of 15 patients with TTP-D ≥2 seconds, CBF/CBV was abnormally reduced. The cutoff of TTP-D at 2 seconds provided high specificity (72%, 43/60 ROIs; 78%, 7/9 patients) and good sensitivity (81%, 65/80 ROIs; 87%, 13/15 patients) for assessing abnormal reduction of CBF/CBV.

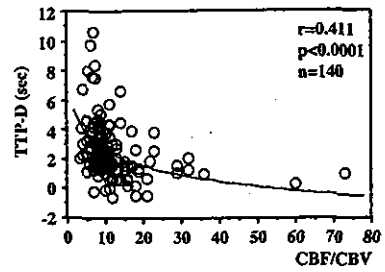

Figure 3. Relation between TTP-D and CBF/CBV in 140 ROIs. A significant correlation is observed between the 2 parameters (r=0.441; P<0.001; n=140).

In the analysis of all 140 ROIs, TTP-D correlated significantly with OEF (r=0.576, P<0.0001). However, in the analysis of 60 ROIs with normal CBF/CBV alone, TTP-D showed no significant correlation with OEF. In the analysis of 80 ROIs with reduced CBF/CBV alone, a strong positive correlation was observed between TTP-D and OEF (r=0.710, P<0.0001) (Figure 5). TTP-D in group β was significantly longer than that in group α (4.8±2.2 versus 2.0±0.9 seconds; P<0.01) (Figure 4B). In 5 patients with TTP-D ≥4 seconds, OEF was elevated to an abnormal extent. The cutoff of TTP-D at 4 seconds provided good specificity (96%, 108/112 ROIs; 100%, 18/18 patients) and high sensitivity (79%, 22/28 ROIs; 83%, 5/6 patients) for evaluating elevated OEF. There was no difference in TTP-D between the patients with anterograde collateral circulation and those with retrograde circulation.

Discussion

In this study we evaluated the usefulness of TTP-D measurements by PWI as a tool of cerebral hemodynamic estimation

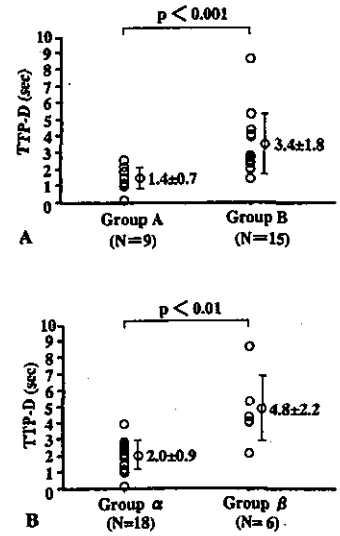

Figure 4. Comparisons of TTP-D between groups with normal CBF/CBV and reduced CBF/CBV (A) and between groups with normal OEF and elevated OEF (B). A, TTP-D in group B (reduced CBF/CBV; n=15) is significantly longer than that in group A (normal CBF/CBV; n=9). B, TTP-D in group β (elevated OEF; n=6) is significantly longer than that in group α (normal OEF; n=18).

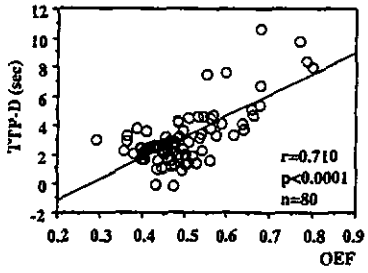

Figure 5. Relation between TTP-D and OEF in 80 ROIs with reduced CBF/CBV. A significant positive correlation is found between the 2 parameters (r=0.710, P<0.0001; n=80).

in patients with unilateral occlusive carotid disease. TTP-D correlated significantly with PET parameters, such as CBF/CBV and OEF. TTP maps are often used for volumetric analyses because the mappings can demonstrate areas of perfusion deficits most distinctively. TTP values, however, are difficult to compare between individuals because the time from the intravenous injection to the bolus arrival at the cerebral arteries varies greatly between patients.[16] Our approach to circumvent this problem was to calculate TTP-D; this is achieved simply by subtracting the bolus arrival time in the contralateral hemisphere from that in the occluded hemisphere. If done in a standardized fashion, the interobserver agreement of this method is good and requires minimal postprocessing.

Quantitative evaluations of CBF and CBV are enabled by PWI with the use of various techniques, such as the indicator dilution method with AIF or the arterial spin labeling method.[2-6,17] The former method requires determination of AIF and subsequent deconvolution techniques demanding a high level of operator intervention and relatively time-consuming postprocessing. Furthermore, it remains controversial whether ICA or MCA is more suitable as a source of AIF. In addition to the shape of the injected bolus, AIF depends on cardiac output, vascular geometry, and cerebral vascular resistance. The latter method, arterial spin labeling, was confirmed to be useful for evaluating the hemodynamics in acute stroke because the results obtained are potentially quantitative.[18] However, there are still technical problems to be solved in this technique. The main advantages of using TTP-D to evaluate tissue perfusion are the feasibility of techniques, the requirement of minimal postprocessing time, and the capability of demonstrating abnormal regions distinctively.

Ostergaard et al[5,6] compared absolute CBF and CBV values obtained by PWI and those measured by PET in 6 healthy volunteers and experimental pigs. However, there have been few direct comparisons between PWI and established perfusion imaging techniques in clinical ischemic stroke.[8-10] Kikuchi et al[8] compared CBF and CBV measured by PWI using the indicator dilution method and cerebral perfusion reserve estimated by xenon-133 single-photon emission CT (SPECT) with acetazolamide in 8 patients with chronic occlusive carotid disease. CBF values measured by 2 methods were closely correlated with each other, yet the resolution of PWI was superior to that of SPECT. Furthermore, PWI provided important clinical information for evaluating the degree of perfusion reserve impairment. Barber et al[9] compared hypoperfusion volumes determined by CBF, CBV, and mean transit time maps of PWI and those estimated with ^{99m}Tc–hexamethylpropyleneamine oxime (HMPAO) SPECT in 17 chronic stroke patients. PWI maps were found to delineate peri-infarct hypoperfusion areas similar to ^{99m}Tc-HMPAO SPECT. Hagen et al[10] compared CBF measured by PWI and xenon CT in 10 patients. CBF values measured by the 2 methods were closely correlated with each other, and the resolution of PWI was as high as that of xenon CT. Thus, PWI using the indicator dilution method makes it possible to estimate the degree of hypoperfusion with high reliability. However, no information concerning cerebral metabolism is available with the indicator dilution measurement of PWI.

To the best of our knowledge, there has been no clinical study comparing TTP-D obtained by PWI and PET parameters. Several studies reported that TTP-D measured in the acute phase of stroke correlated well with clinical outcome.[19-21] Beaulieu et al[20] and Neumann-Haefelin et al[21] reported that TTP-D had significant correlations with stroke volume and clinical outcome scores.

In the present study 13 of 15 patients with TTP-D ≥2 seconds showed a reduction of CBF/CBV as estimated by PET. CBF/CBV is a sensitive marker of perfusion pressure[22] and may be reduced even in cases of a modest decrease of perfusion pressure, such as those of the oligemic state. Therefore, TTP-D may be useful for detecting areas of low perfusion pressure that are viable but at risk of infarction.

One of the most reliable indicators of hemodynamic impairment is misery perfusion, which is characterized by elevated OEF with the use of PET. According to a study by Yamauchi et al[23] in 40 patients with symptomatic ICA or MCA occlusive disease, increased OEF was an independent predictor of 5-year risk of subsequent stroke. With our semiquantitative approach, we were able to identify patients with OEF elevation as those with TTP-D ≥4 seconds. The cutoff of TTP-D at 4 seconds provided good specificity (96% for regional values and 100% for mean values) and high sensitivity (79% for regional values and 83% for mean values) for evaluating OEF elevation. These specificity and sensitivity values for the detection of OEF elevation are comparable to those of ^{123}I-iodoamphetamine SPECT. Imaizumi et al[24] studied the capability of split-dose ^{123}I-iodoamphetamine SPECT for detecting OEF elevation in 27 patients with chronic carotid occlusive disease on the basis of comparisons with PET parameters. The specificity and sensitivity for the detection of OEF elevation were 96% and 82%, respectively. Measurements of TTP-D in chronic ischemic stroke therefore may enable detection of patients with a high risk of ischemic stroke and selection of candidates for further investigation of cerebral circulation with considerably high reliability.

There are several limitations of the hemodynamic evaluation with TTP-D. First, TTP-D is a semiquantitative and indirect measure of tissue perfusion that is obtained on the basis of comparison of 2 hemispheric parameters. The existence of occlusive changes in both cerebral hemispheres likely complicates interpretation of results obtained by this method. Therefore, we excluded patients with bilateral ca-

rotid artery diseases from the present study to obtain a simple experimental population. This, however, does not necessarily mean that TTP-D measurement is meaningless in cases of bilateral carotid artery diseases. A similar TTP-D study in patients with bilateral carotid occlusive diseases should be performed in the future to elucidate the validity of TTP-D measurements in bilateral carotid artery diseases. Second, since contrast media must be administered as a bolus, imaging can be performed only once per imaging session in a first-pass bolus study. Therefore, the quality of the study depends on the administration of a bolus, which requires good venous access.

PWI is a reliable and noninvasive method, available even in outpatients, to assess changes in cerebral perfusion with unilateral carotid occlusion. This MR technique permits monitoring of longitudinal hemodynamic changes, while the conventional MR technique provides high-resolution and high-contrast anatomic information simultaneously. TTP-D can be used to select patients who are candidates for extensive evaluation of vascular lesions by conventional angiography and cerebral hemodynamics by SPECT or PET. PWI is noninvasive, is relatively inexpensive compared with PET or SPECT, and is a simple method that requires less than a few minutes of scanning time. If the present findings can be confirmed in a larger patient sample, TTP-D may be used for selection of specific therapy, such as thrombolytic or neuroprotective therapy in acute stroke and extracranial-intracranial bypass surgery in chronic stroke.

Acknowledgments

This work was supported in part by special coordination funds for promoting science and technology from the Science and Technology Agency of Japan and by research grants for cardiovascular disease (14-1) from the Ministry of Health and Welfare of Japan. We thank Reiko Manabe for invaluable secretarial assistance.

References

1. Warach S, Dashe JF, Edelman RR. Clinical outcome in ischemic stroke predicted by early diffusion-weighted and perfusion magnetic resonance imaging: a preliminary analysis. *J Cereb Blood Flow Metab.* 1996;16:53–59.
2. Koshimoto Y, Yamada H, Kimura H, Maeda M, Tsuchida C, Kawamura Y, Ishii Y. Quantitative analysis of cerebral microvascular hemodynamics with T2-weighted dynamic MR imaging. *J Magn Reson Imaging.* 1999;9:462–467.
3. Vonken EJ, van Osch MJ, Bakker CJ, Viergever MA. Measurement of cerebral perfusion with dual-echo multi-slice quantitative dynamic susceptibility contrast MRI. *J Magn Reson Imaging.* 1999;10:109–117.
4. Rempp KA, Brix G, Wenz F, Becker CR, Guckel F, Lorenz WJ. Quantification of regional cerebral blood flow and volume with dynamic susceptibility contrast-enhanced MR imaging. *Radiology.* 1994;193:637–641.
5. Ostergaard L, Johannsen P, Host-Poulsen P, Vestergaard-Poulsen P, Asboe H, Gee AD, Hansen SB, Cold GE, Gjedde A, Gyldensted C. Cerebral blood flow measurements by magnetic resonance imaging bolus tracking: comparison with [^{15}O]H_2O positron emission tomography in humans. *J Cereb Blood Flow Metab.* 1998;18:935–940.
6. Ostergaard L, Smith DF, Vestergaard-Poulsen P, Hansen SB, Gee AD, Gjedde A, Gyldensted C. Absolute cerebral blood flow and blood volume measured by magnetic resonance imaging bolus tracking: comparison with positron emission tomography values. *J Cereb Blood Flow Metab.* 1998;18:425–432.
7. Ostergaard L, Weisskoff RM, Chesler DA, Gyldensted C, Rosen BR. High resolution measurement of cerebral blood flow using intravascular tracer bolus passages, part I: mathematical approach and statistical analysis. *Magn Reson Med.* 1996;36:715–725.
8. Kikuchi K, Murase K, Miki H, Kikuchi T, Sugawara Y, Mochizuki T, Ikezoe J, Ohue S. Measurement of cerebral hemodynamics with perfusion-weighted MR imaging: comparison with pre- and post-acetazolamide ^{133}Xe-SPECT in occlusive carotid disease. *AJNR Am J Neuroradiol.* 2001;22:248–254.
9. Barber PA, Consolo HK, Yang Q, Darby DG, Desmond PM, Lichtenstein M, Tress BM, Davis SM. Comparison of MRI perfusion imaging and single photon emission computed tomography in chronic stroke. *Cerebrovasc Dis.* 2001;11:128–136.
10. Hagen T, Bartylla K, Piepgras U. Correlation of regional cerebral blood flow measured by stable xenon CT and perfusion MRI. *J Comput Assist Tomogr.* 1999;23:257–264.
11. Whisnant JP, Basford JR, Bernstein EF, Cooper ES, Dyken ML, Easton JD, Little JR, Marler JR, Millikan CH, Petito CK, et al. Classification of cerebrovascular diseases III. *Stroke.* 1990;21:637–676.
12. Calamante F, Ganesan V, Kirkham FJ, Jan W, Chong WK, Gadian DG, Connelly A. MR perfusion imaging in moyamoya syndrome: potential implications for clinical evaluation of occlusive cerebrovascular disease. *Stroke.* 2001;32:2810–2816.
13. Frackowiak RS, Lenzi GL, Jones T, Heather JD. Quantitative measurement of regional cerebral blood flow and oxygen metabolism in man using ^{15}O and positron emission tomography: theory, procedure, and normal values. *J Comput Assist Tomogr.* 1980;4:727–736.
14. Martin WR, Powers WJ, Raichle ME. Cerebral blood volume measured with inhaled C^{15}O and positron emission tomography. *J Cereb Blood Flow Metab.* 1987;7:421–426.
15. Hirano T, Minematsu K, Hasegawa Y, Tanaka Y, Hayashida K, Yamaguchi T. Acetazolamide reactivity on ^{123}I-IMP single photon emission computed tomography in patients with major cerebral artery occlusive disease: correlation with positron emission tomography parameters. *J Cereb Blood Flow Metab.* 1994;14:763–770.
16. Calamante F, Gadian DG, Connelly A. Delay and dispersion effects in dynamic susceptibility contrast MRI: simulations using singular value decomposition. *Magn Reson Med.* 2000;44:466–473.
17. Ernst T, Chang L, Itti L, Speck O. Correlation of regional cerebral blood flow from perfusion MRI and SPECT in normal subjects. *Magn Reson Imaging.* 1999;17:349–354.
18. Siewert B, Schlaug G, Edelman RR, Warach S. Comparison of EPISTAR and T2'-weighted gadolinium-enhanced perfusion imaging in patients with acute cerebral ischemia. *Neurology.* 1997;48:673–679.
19. Tong DC, Yenari MA, Albers GW, O'Brien M, Marks MP, Moseley ME. Correlation of perfusion- and diffusion-weighted MRI with NIHSS score in acute (<6.5 hour) ischemic stroke. *Neurology.* 1998;50:864–870.
20. Beaulieu C, de Crespigny A, Tong DC, Moseley ME, Albers GW, Marks MP. Longitudinal magnetic resonance imaging study of perfusion and diffusion in stroke: evolution of lesion volume and correlation with clinical outcome. *Ann Neurol.* 1999;46:568–578.
21. Neumann-Haefelin T, Wittsack HJ, Wenserski F, Siebler M, Seitz RJ, Modder U, Freund HJ. Diffusion- and perfusion-weighted MRI: the DWI/PWI mismatch region in acute stroke. *Stroke.* 1999;30:1591–1597.
22. Schumann P, Touzani O, Young AR, Baron JC, Morello R, MacKenzie ET. Evaluation of the ratio of cerebral blood flow to cerebral blood volume as an index of local cerebral perfusion pressure. *Brain.* 1998;121:1369–1379.
23. Yamauchi H, Fukuyama H, Nagahama Y, Nabatame H, Ueno M, Nishizawa S, Konishi J, Shio H. Significance of increased oxygen extraction fraction in five-year prognosis of major cerebral arterial occlusive diseases. *J Nucl Med.* 1999;40:1992–1998.
24. Imaizumi M, Kitagawa K, Hashikawa K, Oku N, Teratani T, Takasawa M, Yoshikawa T, Rishu P, Ohtsuki T, Hori M, et al. Detection of misery perfusion with split-dose ^{123}I-iodoamphetamine single-photon emission computed tomography in patients with carotid occlusive diseases. *Stroke.* 2002;33:2217–2223.

Available online at www.sciencedirect.com
SCIENCE DIRECT
Neuroscience Research 46 (2003) 281–288
Neuroscience Research
www.elsevier.com/locate/neures

Magneto-encephalographic measurement of neural activity during period of vertigo induced by cold caloric stimulation

Akihiko Kandori [a,*], Hiroshi Oe [b], Kotaro Miyashita [b], Shinji Ohira [b], Hiroaki Naritomi [b], Yoshihide Chiba [b], Kuniomi Ogata [a], Masahiro Murakami [c], Tsuyoshi Miyashita [a], Keiji Tsukada [a]

[a] *Medical System Research Department, Central Research Laboratory, Hitachi, Ltd., 1-280 Higashi-Koigakubo, Kokubunji-shi, Tokyo 185-8601, Japan*
[b] *National Cardiovascular Center, 5-7-1 Fujishirodai, Suita, Osaka 565-8565, Japan*
[c] *Instruments, Hitachi, Ltd., 882 Ichige, Hitachinaka-shi, Ibaraki 312-8504, Japan*

Received 27 November 2002; accepted 18 February 2003

Abstract

The aim of this study was to investigate neural activity during period of vertiginous sensation, induced by caloric stimulation. After caloric vestibular stimulation (CVS) by cold water of five volunteers ($n=5$, age: 30 ± 10), auditory evoked magnetic fields (AEFs) during the subsequent period of vertiginous sensations were measured by magnetoencephalography (MEG). Current-arrow maps (CAMs) were produced to estimate the spatial current distribution of the AEF responses, and a rotation value (dI_{rot}) was calculated from the CAM. The worth of the dI_{rot} values as indicators of vertigo was evaluated by comparing them with earlier reported values for elderly control ($n=11$, age: 67 ± 5) and chronic dizziness (CD) ($n=27$, age: 68 ± 8) groups (obtained from AEF responses with no the CVS). Although all volunteers felt vertigo during the AEF measurements, the AEF waveforms and CAM pattern only showed slight changes. While the dI_{rot} values (1.43 ± 0.73) just after CVS were not significantly different from those (1.59 ± 0.46) for the elderly controls, they were significantly different from those (3.54 ± 1.34) for the CD patients. These findings suggest that (i) the new parameter (dI_{rot}) is more sensitively indicates dizziness (non-rotatory sensation) than vertigo (ii) the auditory cortical region may play an important role in body-balance perception of floating sensations.

Keywords: Vertigo; Dizziness; Caloric vestibular stimuli; Magnetoencephalogram; Vestibular function; Auditory cortical function; Current-arrow map

1. Introduction

Many people, particularly among the elderly, commonly complain of dizziness (non-rotatory sensations) and vertigo (rotatory sensations), which are caused by many different patho-physiological mechanisms (Baloh, 1995; Grimby and Rosenhall, 1995). Although they are clinically different symptoms, vestibular function has main role in both (Baloh, 1992). Therefore, quantitatively evaluating the difference in neurological activity between the sensations is important.

However, dizziness (non-rotatory sensations) is a difficult symptom to assess because it is a subjective sensation that cannot be measured, and is a nonspecific symptom caused by many different patho-physiological mechanisms (Baloh, 1995). Formby et al. (1988) stimulated a caloric vestibular response by irrigation with cold or hot water as a means for investigating the mechanisms of such sensations in patients. However, they were unable to find evidence of a tonotopic relation between audiometric (hearing loss) and caloric vestibular functions.

On the other hand, many otologists have used caloric-vestibular tests in investigating the mechanism of vertigo. Although the correlation between the caloric vestibular and earth-vertical-rotational responses is not good (Furman and Kamerer, 1989), increased regional

* Corresponding author. Tel.: +81-42-323-1111; fax: +81-42-327-7783.
E-mail address: kandori@crl.hitachi.co.jp (A. Kandori).

0168-0102/03/$ - see front matter
doi:10.1016/S0168-0102(03)00092-0

cerebral blood flow (rCBF) was seen in the superior temporal region posterior to the auditory area during caloric vestibular stimulation (CVS) with warm water (Friberg et al., 1985). Furthermore, positron-emission tomography (Wenzel et al., 1996) and transcranial Doppler sonography (Tiecks et al., 1996) were revealed that caloric irrigation led not only to increased velocity in the middle cerebral artery (MCA) but, at the same time, to decreased velocity in the posterior cerebral artery (PCA). The respective CBF changes reflect activation of the caloric vestibular cortex along with functional deactivation of the visual cortex.

With the above work in mind, we have used magnetoencephalography (MEG) to show that patients with chronic dizziness (CD), which was defined (Oe et al., 2002a) as abnormal feelings of floating, swaying and/or non-rotatory dizziness persisting for more than 6 months, have an abnormal auditory-magnetic-field (AEF) response, in spite of the fact that they were normal in terms of both pure-tone audiogram and auditory brainstem responses (Kandori et al., 2002b; Oe et al., 2002a). We have developed a form of topographic depiction for electrical abnormalities in the brain (Kandori et al., 2002a). The abnormalities of interest here produce a rotational current distribution on the temporal lobe so, we have developed a quantitative method for estimating the degree of rotation, dI_{rot} (Oe et al., 2002a). This method gives us a quantitative measure of sensations of dizziness and of the efficacy of their treatment.

However, whether or not our parameter also reflects vertigo was not clear, and the relation between the auditory cortex and the caloric vestibular cortex, which are close to each other, is also open to question. To clarify the first point and as a step towards understanding the relation between the auditory cortex and the caloric vestibular cortex, we have now measured the AEF signal during the post-CVS period of vertiginous sensations.

2. Method

2.1. Subjects

The subjects were five normal volunteers (two males and three females, age: 30 ± 10) with no history of acoustic problems. As comparative data on CD cases, we used previously reported data on 27 elderly patients with CD (13 males and 14 females, age: 68 ± 8) and 11 other elderly subjects (four males and seven females, age: 67 ± 5) with no history of acoustic problems (Oe et al., 2002a). Here, CD was defined as abnormal feelings of floating, swaying and/or non-rotatory dizziness persisting for more than 6 months (see Oe et al., 2002a).

2.2. MEG measurements

We used a superconducting quantum interference device (SQUID)-based system (Hitachi, Ltd.), a 64 element coaxial-gradiometer array (Kandori et al., 2001) to measure auditory evoked magnetic fields (AEFs). This system was installed in a magnetically shielded room (MSR) with walls made of a double layer of mumetal. The array of SQUID-based sensors is an 8×8 matrix (with a pitch of 25 mm) on a flat plane. Each sensor incorporates a first-order gradiometer that includes an 18-mm-diameter bobbin with a 50-mm-long baseline. The magnetic field sensitivities of all channels are below 20 fT $Hz^{-1/2}$. The AEF signals of the five volunteers (age: 30 ± 10) were measured three times (before the CVS, 2–4 min after the CVS, and 4–6 min after the CVS; see Fig. 1) from the left hemisphere of each volunteer. The anatomical head position was adjusted according to four coil indicators on an orbitomeatal basal (OM) line. After being passed through a bandpass filter (0.1–50 Hz), notch filter (50 Hz), and amplifier circuit, the AEF signals (2 min) from the left hemisphere were digitized at 1 kHz by computer. The AEF was obtained by passing a burst of sound (1 kHz, 90 dB, center stimulus frequency: 0.7 Hz) through the MSR from the outside. In each 2-min AEF term, an AEF signal averaged over 100 epochs was calculated. The highest-amplitude waveform was defined as the N100m (Kandori et al., 2002b; Oe et al., 2002b), and the current distribution at the corresponding time was analyzed. Informed consent for these measurements, was obtained from all of the volunteers.

2.3. Procedure for caloric vestibular stimulation

Before CVS, an otolaryngologist must verify that the ear canal is clear and the drum is intact. Subjects reclined in the supine position, their head slightly elevated, by approximately 30° so that the lateral canal was aligned with the gravitational vertical. The right-ear canal was stimulated by irrigation with open-loop water, i.e. 5 ml of cold (5 °C) water (see lower part of Fig. 1). This stimulation was applied for about 30 s. The CVS was administrated corresponding to the correct procedure, along with a routine test, by an experienced otolaryngologist (our co-worker).

Eye movements were measured by means of electronystagmography (ENG) (upper part of Fig. 1). Immediately after confirming subjective dizziness through words and nystagmus by ENG, the acoustic stimulation was delivered through an air-tube earphone to the subject. The AEF signals from the left temporal lobe during the acoustic stimulation were then measured over two periods (2–4 and 4–6 min), because the dizzy sensation decreased and disappeared within 6 min and the two periods represent stronger and weaker sensa-

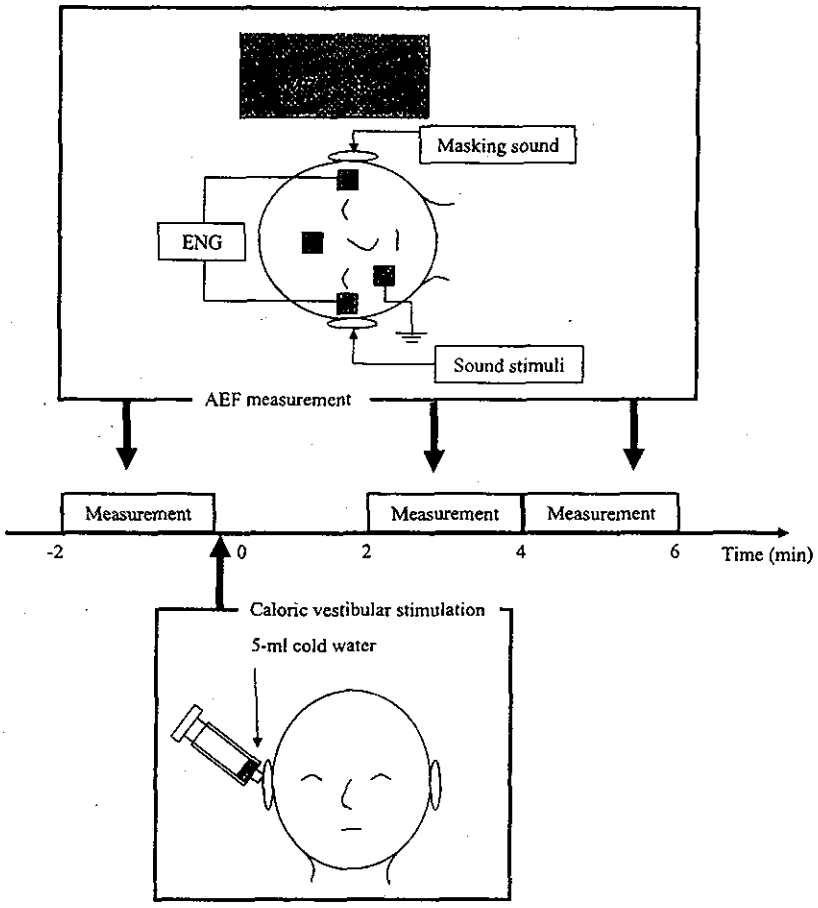

Fig. 1. Protocol and procedure for AEF and ENG measurement and CVS. In the three AEF measurements (2 min), a sound stimuli was delivered to the right ear of each subject, with the ENG signal between the left side of the left eye and the right side of the right eye simultaneously recorded. CVS was performed by irrigating the right ear with cold water (5 °C).

tions. For the CVS test, informed consent of all volunteers was obtained. We decided that the local ethical committee's approval of this procedure was not necessary, because the CVS test (as used in this study) is used in routine examinations and an otolaryngologist checked the ear canals and drums of the subjects before and after the procedure.

2.4. Calculation of dI_{rot}

Our MEG system can produce current-arrow map (CAM), which provides a visual depiction of pseudo-current patterns in the brain, from the derivatives of the normal component (Bz) of N100m in the AEF signals (Kandori et al., 2002a) given as:

$$Ix = dBz/dy \quad (1)$$

and

$$Iy = -dBz/dx. \quad (2)$$

The magnitude of the current arrows $I = (Ix^2 + Iy^2)^{1/2}$ is then plotted as a contour map.

A rotation map is produced to quantitatively evaluate the electrical rotational directions of current arrows on the CAM (Fig. 2a). To make this map, the positive direction for current paths is defined as counter-clockwise (Fig. 2b). Therefore, clockwise arrows show a negative value and counter-clockwise arrows indicate a positive value. We resolved the four current arrows (I_1, I_2, I_3, and I_4) on the rotation pathway (Fig. 2c) at each position from the direction of the arrow at that position and its adjacent arrows; we then calculated the sum of the four current arrows ($I_1+I_2+I_3+I_4$). From such sums, we can obtain a rotation map (Fig. 2d). For example, in a normal subject (Fig. 2d), clockwise arrows are depicted as the positive values (continuous lines) and counter-clockwise arrows are depicted as the negative values (dotted lines). Finally, to express the rotation characteristic in a single quantity, we calculated the absolute differences (dI_{rot}) between the maximum positive and minimum negative values (Fig. 2e). In the case of a normal subject (Fig. 2d), dI_{rot} is nearly zero because the negative and positive peaks of one dipole pattern have almost the same magnitudes. However, if one of

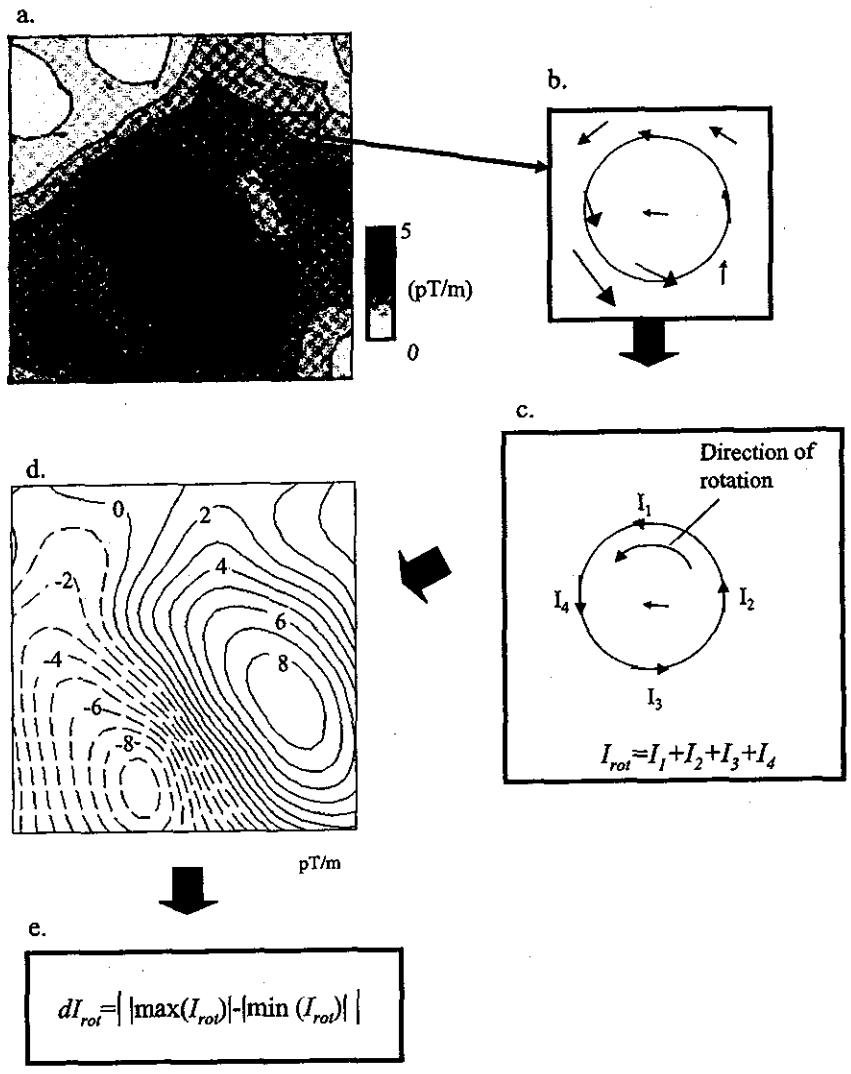

Fig. 2. Method for calculation of dI_{rot} values: (a) CAM, (b) sample of current arrows, (c) rotation direction for summation ($I_{rot} = I_1+I_2+I_3+I_4$), (d) rotation map, and (e) subtraction of minimum from maximum absolute value of I_{rot}.

the two rotation pathways is larger than the other (as is the case in, e.g. CD patients), the difference between the two values will be larger.

The dI_{rot} values of the volunteers were compared with the values for the elderly people, both the control subjects and CD patients, which were previously reported (Oe et al., 2002a). Note that these earlier reported values were obtained with no CVS by using the N100m.

3. Results

ENG waveforms and acoustic timing during the AEF measurements are shown in Fig. 3: (a) before CVS; (b) 2–4 min after CVS. The nystagmic direction is given to right of the ENG waveform. The nystagmic responses are greater before than after CVS, and occur randomly against the acoustic stimuli timing. All five volunteers fully felt a rotational sensation due to the CVS. While all subjects claimed a vertiginous sensation, we defined two claim groups; subjects in one group claimed strong nausea, while those in the other claimed mild nausea.

Typical signals and CAMs from a volunteer who experienced a strong vertiginous sensation are shown in Fig. 4(a) before and (b) after caloric irrigation. The signals are the AEF and ENG as averaged by using the acoustic stimulation trigger. The CAMs are for N100m, which is the highest magnitude in the AEF waveforms. Flat ENG waveforms can be seen in both figures. The difference between the AEF signals and CAMs before and after CVS is slight, in spite of the subject's sensation of rotation.

The quantitative values, dI_{rot}, before and after the CVS are shown in Fig. 5. Results for the three volunteers (open circles) with the stronger induced

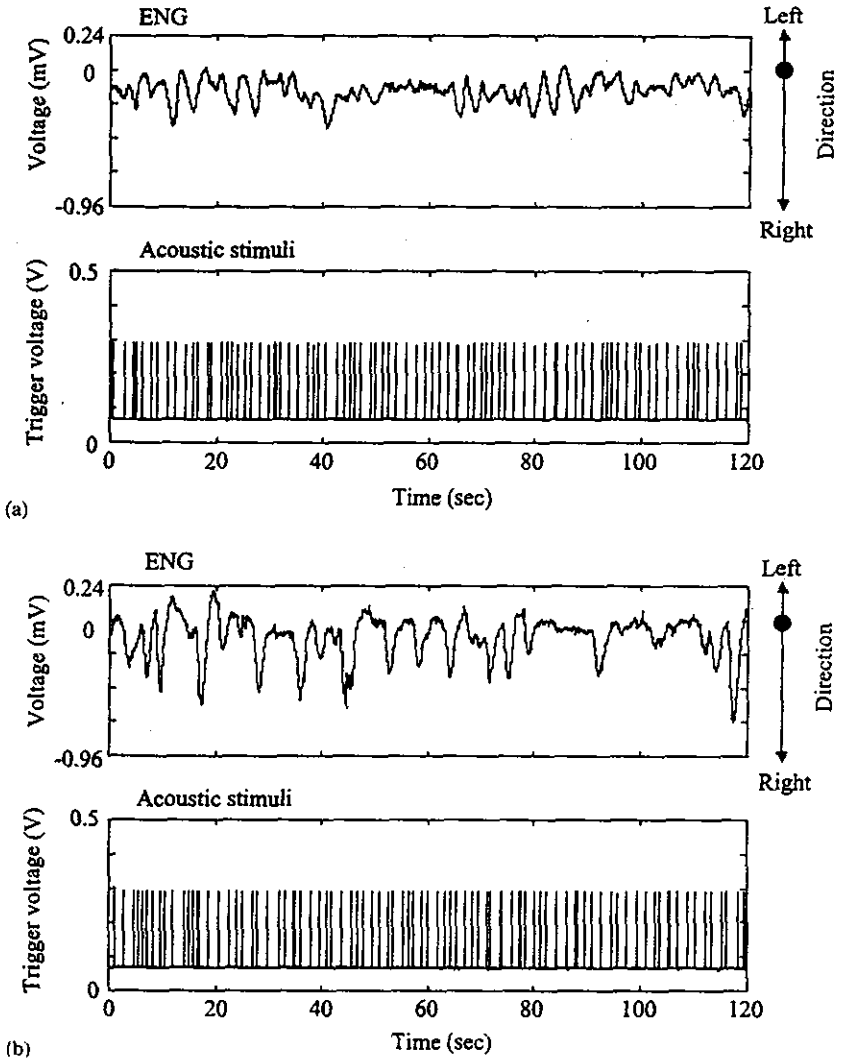

Fig. 3. Raw ENG signals and acoustic stimuli-trigger signals: (a) before and (b) 2–4 min after CVS. Cold water irrigation evokes a rightward movement of the eye.

vertiginous sensation (stronger nausea) show a tendency for dI_{rot} to increase just after CVS. However, the highest value of the open circles is still within the earlier reported range for normal elderly subjects (Oe et al., 2002a). On the other hand, values (solid circles) for the two volunteers who only experienced mild dizziness showed no change during the measurements.

The statistically analyzed dI_{rot} values are listed in Tables 1 and 2. Table 1 indicates the difference between dI_{rot} before and after CVS for each of the two volunteer groups (strongly and mildly dizzy), and Table 2 shows the differences between volunteer groups, the normal elderly control groups, and elderly CD patients. In Table 1, although there is a clear difference between the dI_{rot} values before CVS and 2–4 min after CVS in the case of strong-dizziness volunteers, this is not the case for the mild-dizziness pair. In Table 2, the dI_{rot} values under each of the three time conditions for all volunteers and for patients with CD are significantly different. However, the dI_{rot} values for the normal elderly control group are significantly different from those of the volunteers both before CVS and 4–6 min after CVS.

4. Discussion

The large right-ward motion of the eyes in Fig. 3 shows that cold-water irrigation of the right ear affected the vestibular function. Since sufficient stimulation could lead to artifacts through eye movement, the raw ENG signals were averaged to investigate the artifact (Fig. 4). The averaged ENG signal thus obtained

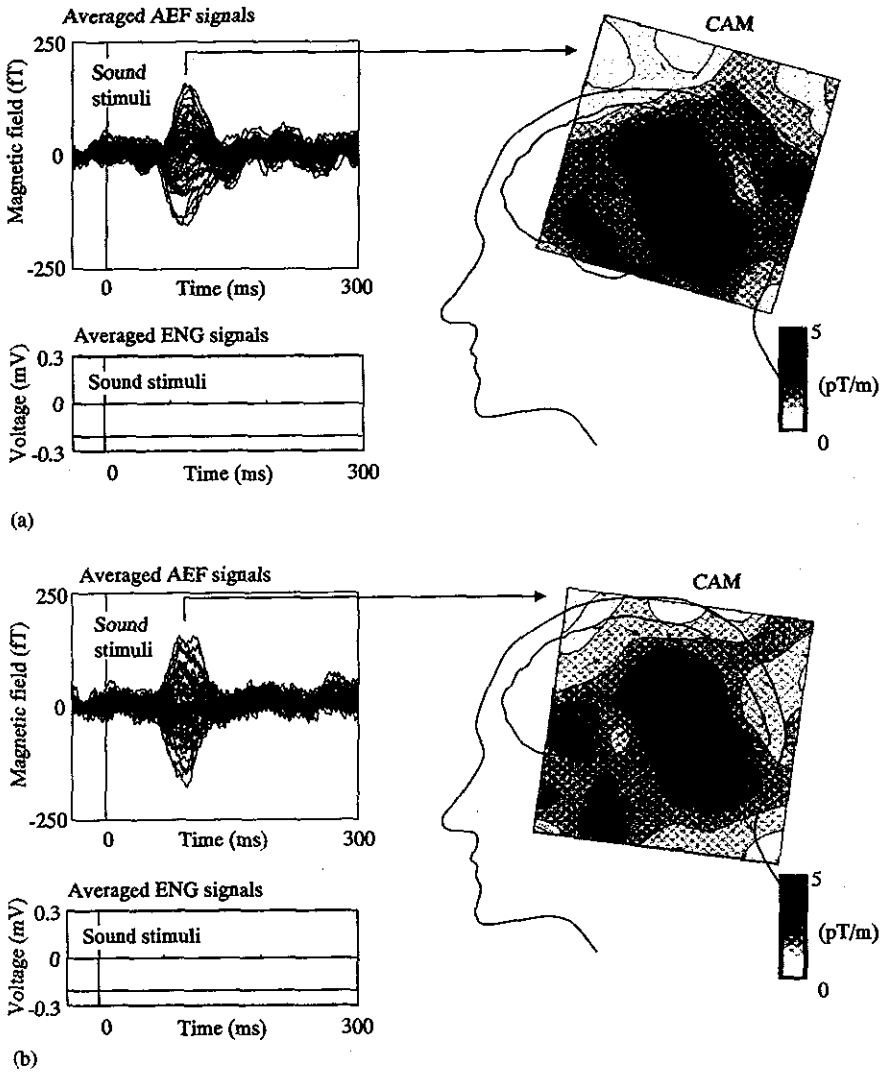

Fig. 4. Typical averaged AEF and ENG waveforms and CAMs: (a) before and (b) 2–4 min after CVS. The CAMs were produced at the N100m peak and superimposed on the outline of a brain and head by using the OM line. There are only slight differences between the AEF results and CAMs before and after CVS. The averaged ENG signals show a flat line, which indicates an absence of artifacts from the AEF signals.

appears flat; therefore, we can conclude that there is no artifact due to CVS in the averaged AEF waveforms. Furthermore, the fact that all five volunteers felt a rotational sensation due to the CVS indicates that, the CVS was strong enough to elicit severe vertigo with a nystagmic response. Although the presence of water in the canal around the drum may have a small effect on the auditory input, this effect could not be a serious problem because all of the volunteers rated their auditory perception as normal.

In Fig. 5 and Table 1, we see that the dI_{rot} values provide a quantitative evaluation of the vertiginous sensation in those cases where strong vertigo was felt; that is, the strongest vertigo appeared 2–4 min after CVS. However, even the largest value is within the range for the elderly control subjects, and the values for volunteers with mild vertigo are not significantly different. This suggests that CVS hardly affects the auditory cortical function in spite of the reduced the CBF in the MCA (Wenzel et al., 1996; Tiecks et al., 1996).

Table 2 indicates that there is a difference between the caloric vestibular and auditory cortical functions, because the dI_{rot} values after CVS are significantly lower than the values for the CD patients. This finding suggests abnormalities in the auditory cortices of the elderly dizzy patients with high dI_{rot} values, since these data were calculated by using the AEF data measured during auditory cortical stimulation only (i.e. with no CVS). The neural activity seen with vertigo due to CVS

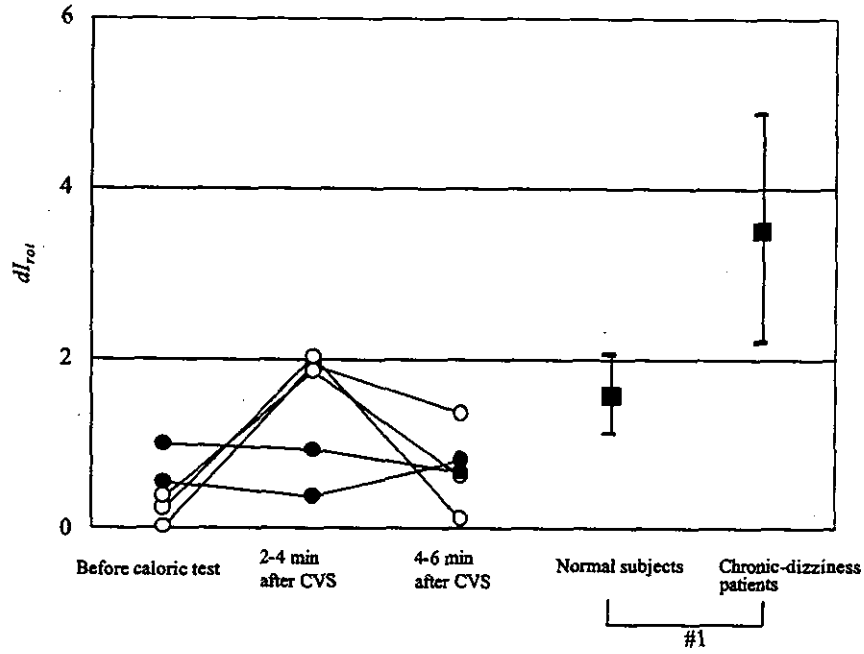

Fig. 5. Variation of dI_{rot} values with caloric stimulus and time; results for age-matched groups of elderly subjects with and without dizziness (rotatory sensations). Open circles indicate values for the three volunteers with strong vertigo and closed (solid) circles indicate values for the two volunteers with mild vertigo. The plots (mean value and standard deviation) labeled #1 are obtained from previously published data (Oe et al., 2002a).

Table 1
Values for dI_{rot} before and in two periods after caloric stimuli by volunteer group (strong ($n=3$) and mild ($n=2$) vertigo)

	Before CVS	2–4 min after CVS	4–6 min after CVS
Volunteers with strong dizziness ($n=3$)	0.22±0.17	1.94±0.09	0.71±0.63
Volunteers with mild dizziness ($n=2$)	0.77±0.32	0.66±0.38	0.74±0.10

CVS, caloric vestibular stimuli.

Table 2
Values for dI_{rot} of the volunteer group ($n=5$, age: 30±10), normal elderly control subjects ($n=11$, age: 67±5), and elderly CD patients ($n=27$, age: 68±8)

All volunteers (n=5)			Normal elderly	Elderly patients
Before CVS	2-4 min after CVS	4-6 min after CVS	controls (n=11)	with CD (n=27)
0.44±0.36	1.43±0.73	0.72±0.45	1.59±0.46	3.54±1.34

P<0.05 (Before CVS – 2-4 min after CVS)
N.S (2-4 min after CVS – 4-6 min after CVS)
P<0.05 (4-6 min after CVS – Normal elderly controls)
P<0.05 (Normal elderly controls – Elderly patients with CD)
P<0.05 (2-4 min after CVS – Elderly patients with CD)
P<0.05 (Before CVS – Elderly patients with CD)

The average age of the volunteers is very different from that of the elderly people. The latter two sets of values are obtained from previously published work (Oe et al., 2002a). The P values were calculated by Levene's t-test. CVS, caloric vestibular stimuli; CD, chronic dizziness.

is different from that seen in cases of CD. This supports the notion that the auditory cortical region has some function to do with a subjective sensation of floating or subjective spatial balance (Oe et al., 2002a). The existence of some form of balance perception in the auditory cortex was revealed by direct electrical stimulation of the brain (Penfield and Perot, 1963). Electrical stimulation of the auditory region caused a floating

sensation. The results of recent work with direct electrical stimulation have suggested that out-of-body experiences may be the result of failures to integrate complex somatosensory and vestibular information (Blanke et al., 2002). In the case of the CD patients, the main informational failure may lie in abnormal neural activity in relation to the perception of floating in the auditory cortex. Furthermore, abnormal auditory responses may propagate from the temporal cortical area to the vicinity of the auditory cortical region, because the abnormalities in AEF response were characterized by a rotational current distribution in the temporal lobe (Kandori et al., 2002b; Oe et al., 2002a). We can thus conclude that the main cause of the dizzy feeling in CD is a dysfunction of the balance perception mechanism in the auditory cortex.

In Table 2, we see a significant difference between results for the young volunteers (age: 30 ± 10) and the old controls (age: 67 ± 5). This finding suggests that balance perception changes with age. This may be why dizziness and/or vertigo are very common among old people, affecting in about one third of them (Grimby and Rosenhall, 1995).

5. Limitations of this study

Several limitations applied to this study. Firstly, MEG signals from a lot more volunteers will be needed before we can fully evaluate the difference between caloric and CD. Secondly, CAM has a limitation in that it does not express the actual current distribution in the brain. While the present study is methodologically simple and the results are preliminary because of the above limitations, its findings are a step towards a better understanding of the mechanisms of dizziness and vertigo.

Acknowledgements

This study was supported by Grant-in-Aid for Scientific Research No. 13072601 from the Ministry of Health, Labour and Welfare of Japan.

References

Baloh, R.W., 1992. The dizzy patient: treatment options. In: Hachinski, V.C. (Ed.), Challenges in Neurology. FA Davis, Philadelphia, pp. 15–28.

Baloh, R.W., 1995. Approach to the evaluation of the dizzy patients. Otolaryngol. Head Neck Surg. 112, 3–7.

Blanke, O., Origue, S., Landis, T., Seeck, M., 2002. Stimulating illusory own-body perceptions – the part of the brain that can induce out-of-body experiences has been located. Nature 419, 269.

Formby, C., Hixson-Robles, C., Singleton, G.T., 1988. Correlations between hearing thresholds and caloric responses among a heterogeneous sample of dizzy patients. J. Speech Hear. Disord. 53, 65–70.

Friberg, L., Olsen, T.S., Roland, P.E., Paulson, O.B., Lassen, N.A., 1985. Focal increase of blood flow in the cerebral cortex of man during vestibular stimulation. Brain 108, 609–623.

Furman, J.M.R., Kamerer, D.B., 1989. Rotational responses in patients with bilateral caloric reduction. Acta Otolaryngol. (Stockholm) 108, 355–361.

Grimby, A., Rosenhall, U., 1995. Health-related quality of life and dizziness in old age. Gerontology 41, 289–298.

Kandori, A., Kanzaki, H., Miyatake, K., Hashimoto, S., Itoh, S., Tanaka, N., Miyashita, T., Tsukada, K., 2001. A method for detecting myocardial abnormality by using a total current-vector calculated from ST-segment deviation of a magnetocardiogram signal. Med. Biol. Eng. Comput. 39 (1), 21–28.

Kandori, A., Oe, H., Miyashita, K., Date, H., Yamada, N., Naritomi, H., Chiba, Y., Murakami, M., Miyashita, T., Tsukada, K., 2002a. Visualization method of spatial interictal discharges in temporal epilepsy patients by using magnetoencephalogram. Med. Biol. Eng. Comput. 40 (3), 327–331.

Kandori, A., Oe, H., Miyashita, K., Date, H., Yamada, N., Naritomi, H., Chiba, Y., Miyashita, T., Tsukada, K., 2002b. Abnormal auditory-nerve pathways in patients with right hemispheric infarction, chronic dizziness, and moyamoya disease: a magnetoencephalogram study. Neurosci. Res. 44 (3), 273–283.

Oe, H., Kandori, A., Murakami, M., Miyashita, K., Tsukada, K., Naritomi, H., 2002a. Cortical functional abnormality assessed by auditory-evoked magnetic fields and therapeutic approach in patients with chronic dizziness. Brain Res. 957 (2), 373–380.

Oe, H., Kandori, A., Yamada, N., Miyashita, T., Tsukada, K., Naritomi, H., 2002b. Interhemispheric connection of auditory neural pathways assessed by auditory evoked magnetic fields in patients with fronto-temporal lobe infarction. Neurosci. Res. 44 (4), 483–488.

Penfield, W., Perot, P., 1963. The brain's record of auditory and visual experience. Brain 86, 593–696.

Tiecks, F.P., Planck, J., Haberl, R.L., Brandt, T., 1996. Reduction in posterior cerebral artery blood flow velocity during caloric vestibular stimulation. J. Cereb. Blood Flow Metab. 16-6, 1379–1381.

Wenzel, R., Bartenstein, P., Dieterich, M., Danek, A., Weindl, A., Minoshima, S., Ziegler, S., Schwaiger, M., Brandt, T., 1996. Deactivation of human visual cortex during involuntary ocular oscillations. Brain 119, 101–110.

□ ORIGINAL ARTICLE □

Clinical and Radiographic Features of Lobar Cerebral Hemorrhage: Hypertensive Versus Non-hypertensive Cases

Ryo OHTANI, Seiji KAZUI, Hidekazu TOMIMOTO*, Kazuo MINEMATSU and Hiroaki NARITOMI

Abstract

Objectives **The underlying cause of lobar intracerebral hemorrhage (ICH) is often difficult to determine, since these vascular abnormalities are not necessarily visualized in radiographic studies. We sought to determine the clinical features of hypertensive and non-hypertensive lobar ICH, and further predict the presence or absence of vascular abnormalities in terms of clinical features and radiographic abnormalities.**

Patients and Methods **Eighty-one patients with lobar ICH were retrospectively assigned to either hypertensive or non-hypertensive groups based on their blood pressure levels during the chronic phase or a history of antihypertensive medication. The clinical and radiographic features of these two groups were compared.**

Results **Forty-nine patients (60%) were hypertensive, and the other thirty-two (40%) were non-hypertensive. In the non-hypertensive group, amyloid angiopathy (n=6), aneurysms (n=5), arteriovenous malformation (n=4), use of anticoagulants (n=2), liver cirrhosis (n=2) and thrombasthenia (n=1) were found as underlying causes. There were no significant differences between these two groups in the frequencies of stroke risk factors except for hypertension, clinical features and initial neurological findings. On the contrary, subarachnoid extension of the hematoma on CT was significantly more frequent in the non-hypertensive lobar ICH group than in the hypertensive group ($p<0.001$). The patients with subarachnoid extension were more likely to have vascular abnormality than those without subarachnoid extension ($p<0.01$).**

Conclusion **Subarachnoid extension of the hematoma on CT strongly indicates a non-hypertensive cause, and more specifically, it suggests lobar ICH caused by vascular abnormalities.**

(Internal Medicine 42: 576–580, 2003)

Key words: hypertension, lobar hemorrhage, computed tomography, subarachnoid extension, vascular abnormality

Introduction

Hypertension is a relatively infrequent cause of lobar intracerebral hemorrhage (ICH), compared to ICH in the deep regions such as the putamen, thalamus, cerebellum and pons (1). Indeed, lobar ICH is the result of other heterogeneous causes, including arteriovenous malformation, cavernous angioma, aneurysm, brain tumors, especially those of metastatic origin (2, 3), the use of anticoagulant or fibrinolytic agents, cerebral amyloid angiopathy and vasculitis (2). Furthermore, the frequency of lobar ICH complicated by amphetamines (4), pseudoephedrine (5), and cocaine (6) has increased recently. Other relatively rare causes may include moyamoya disease (7), disseminated intravascular coagulation or sepsis (8), cerebral venous thrombosis (9) and leptomeningeal anastomosis after the occlusion of major cerebral artery (10).

Lobar ICH is not necessarily rare, however, there are relatively few studies on lobar ICH in comparison with deep ICH in the thalamus, putamen, pons or cerebellum. In addition, it is often difficult to determine the underlying causes, since vascular abnormalities such as arteriovenous malformation, cavernous angioma or aneurysm are not necessarily visualized in radiological studies. In the present study, we compared the clinical features of hypertensive and non-hypertensive lobar ICH, and further sought to predict the presence or absence of vascular abnormalities in terms of clinical features and CT findings of hematomas.

From the Department of Cerebrovascular Medicine, National Cardiovascular Center, Osaka and *the Department of Neurology, Faculty of Medicine, Kyoto University, Kyoto

Received for publication August 28, 2002; Accepted for publication March 14, 2003

Reprint requests should be addressed to Dr. Ryo Ohtani, the Department of Neurology, Faculty of Medicine, Kyoto University, 54 Shogoin, Kawahara-cho, Sakyou-ku, Kyoto 606-8507

Materials and Methods

We retrospectively reviewed the records of 409 patients with ICH who had been admitted to our stroke care unit from January 1, 1985 to December 31, 1996. Among these patients, 81 were diagnosed with lobar ICH based on their CT findings. They consisted of 56 men and 25 women, and their mean age was 63±13 years (mean±SD). Cerebral angiographic studies were performed in 52 patients. Magnetic resonance imaging (MRI) and magnetic resonance angiography (MRA) were performed in 76 patients and CT angiography (CTA) was performed in 9 patients. These patients were classified into two groups based on the presence or absence of hypertension in the chronic phase. Hypertension was defined to be present if patients fulfilled at least one of the following criteria: 1) a history of antihypertensive medication, 2) a history of hypertension diagnosed by a referring physician or 3) systolic blood pressure greater than 160 mmHg or diastolic blood pressure greater than 95 mmHg on two or more discrete occasions, after 1 month has lapsed from the onset of the ICH.

We then investigated the differences in clinical and radiographic features between the hypertensive and non-hypertensive lobar ICH patients. The variables analyzed included 1) age and gender; 2) probable pathogenesis; 3) location of the hematoma; 4) stroke risk factors including diabetes mellitus, hyperlipidemia, habits of smoking and alcoholic beverage, prior symptomatic stroke or transient ischemic attacks, ischemic heart diseases (myocardial infarction or angina) and hepatic diseases; 5) clinical features at onset such as severe headache, convulsions, vomiting, vertigo or dizziness; 6) initial neurological findings such as the level of consciousness (alert, lethargic, stupor, coma), motor and sensory deficits, dysarthria and aphasia; 7) laboratory findings including fasting blood sugar, hematocrit, platelets, total cholesterol, triglyceride, hemoglobin A1c, prothrombin time, activated partial thromboplastin time, fibrinogen, and fibrin/fibrinogen degradation products; 8) initial CT findings such as hematoma volume (cm^3), ventricular enlargement, mass effect (shift of midline structures or any evidence of herniation) and hematoma extension to the ventricles or subarachnoid space; 9) the duration of admission; and 10) the clinical outcome (modified Rankin scale) (11).

The volume of the ICH was determined in the following manner (12, 13). On the CT slice which shared the largest area of ICH, the largest diameter (A) of the hematoma was measured in centimeters. The second diameter (B) was represented by a line perpendicular to the largest diameter. The height of the hematoma was then calculated by multiplying the number of slices and the slice thickness, thus providing the third diameter (C). These three diameters were multiplied and then divided by 2 (A×B×C/2) to obtain the volume of the ICH. We used the χ^2 test and Student's t test for group comparisons. P values of 0.05 or less were considered to be statistically significant.

Results

Of the 81 patients with lobar ICH, 49 patients were hypertensive (60%) and the other 32 (40%) were non-hypertensive. The hypertensive lobar ICH group consisted of 33 men and 16 women with a mean age of 64±12 years. The non-hypertensive lobar ICH group consisted of 23 men and 9 women with a mean age 63±15 years.

In the non-hypertensive lobar ICH group, 6 patients had cerebral amyloid angiopathy. Four patients were diagnosed by pathological diagnosis and 2 patients were diagnosed on the basis of clinical features (14). Five patients had aneurysms and 4 had arteriovenous malformations, all of which were confirmed by angiographic examinations, MRA and CTA. Two were receiving anticoagulating agents, 2 had liver cirrhosis, 1 had thrombasthenia and 12 had no obvious causes (Table 1). In the hypertensive lobar ICH group, none had these specific causes, except for 2 patients who were receiving anticoagulants.

Hematomas were distributed more commonly in the anterior regions than in the posterior regions in both groups (Table 2). There were no significant differences between the two groups in terms of stroke risk factors, clinical features at onset, initial neurologic findings and clinical outcome. Laboratory examination also revealed no significant differences between the two groups (Table 3).

Table 1. Underlying Causes for Non-hypertensive Lobar Intracerebral Hemorrhage

	Number of patients
Cerebral amyloid angiopathy	6
Aneurysm	5
Arteriovenous malformation	4
Anticoagulant use	2
Liver cirrhosis	2
Thrombasthenia	1
Unknown	12
Total	32

Table 2. Location of the Lobar Intracerebral Hemorrhage

	Hypertensive	Non-hypertensive
Frontal	13 (26.5%)	12 (37.5%)
Temporal	13 (26.5%)	4 (12.5%)
Parietal	8 (16.3%)	6 (18.8%)
Occipital	7 (14.3%)	4 (12.5%)
Fronto-parietal	4 (8.2%)	2 (6.3%)
Fronto-temporal	3 (6.1%)	1 (3.1%)
Parieto-temporal	0 (0%)	2 (6.3%)
Parieto-occipital	1 (2.0%)	1 (3.1%)
Total	49	32

Table 3. Clinical Features of the Lobar Intracerebral Hemorrhage

	Hypertensive (n=49)	Non-hypertensive (n=32)	p value
Stroke risk factors			
Diabetes mellitus	11	4	0.26
Hyperlipidemia	3	2	0.98
Smoking	23	20	0.17
Alcoholic beverage	24	17	0.71
History of cerebral infarction	7	5	0.87
Ischemic heart disease	7	10	0.07
Hepatic disease	8	8	0.34
Clinical features at onset			
Severe headache	27	16	0.65
Seizure or convulsion	9	6	0.97
Vomiting	18	10	0.61
Vertigo or dizziness	2	0	0.25
Initial neurological findings			
Glasgow coma scale	12.7±3.1	12.8±3.0	0.89
Manual muscle strength test			
Upper limb	3.5±1.5	3.6±1.5	0.76
Lower limb	3.6±1.5	3.7±1.5	0.56
Clinical outcome			
Modified Rankin scale	2.4±2.1	2.4±2.3	0.91

In the initial CT findings, there were no significant differences in hematoma volume or in the frequency of ventricular enlargement, mass effect and ventricular extension between the two groups. However, subarachnoid extension was significantly more frequent in the non-hypertensive group (11 out of 32, 34.4%) than in the hypertensive group (2 out of 49, 4.1%) (Table 4). Figures 1A and 1B show representative CT findings of lobar ICH with and without subarachnoid extension, respectively. Of 13 patients with subarachnoid extension, 2 were hypertensive patients and 11 were non-hypertensive patients. In the later, 6 had vascular abnormality (2 with cerebral amyloid angiopathy, 2 with aneurysm and 2 with arteriovenous malformation (Table 5). On the other hand, of 68 patients without subarachnoid extension,

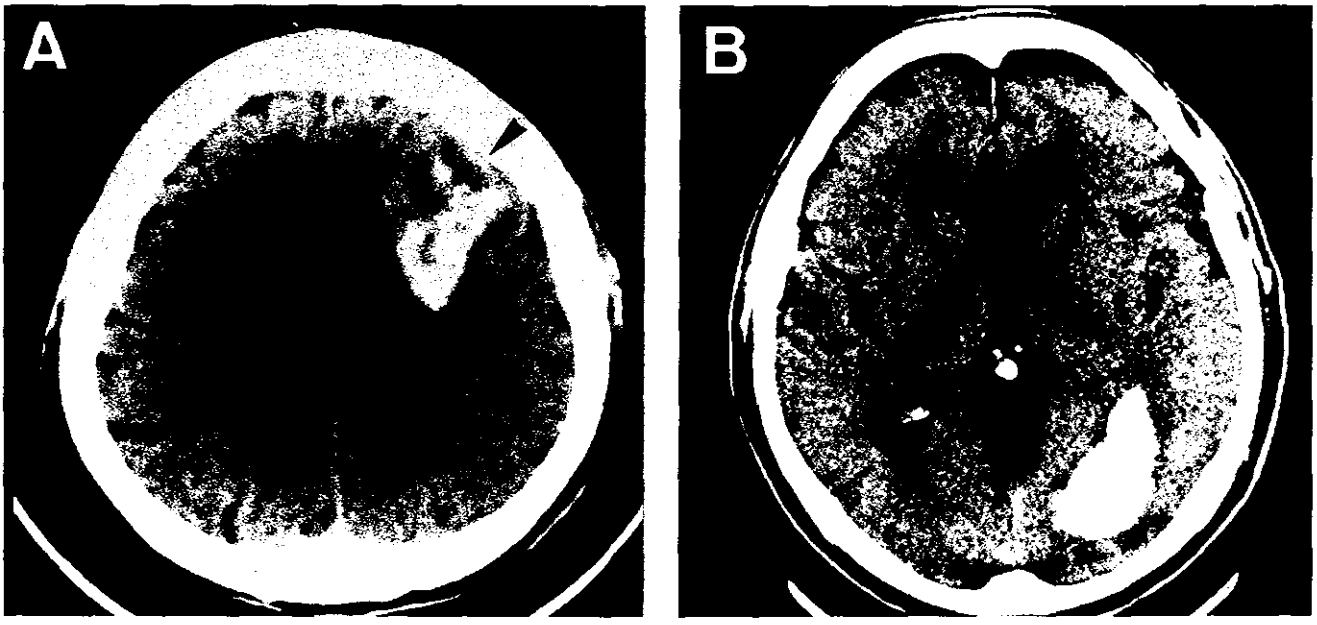

Figure 1. Representative CT findings in patients with and without subarachnoid extension, (A) and (B), respectively. Note extension of the hematoma into the subarachnoid space (arrowhead).